



## OPEN ACCESS

## EDITED BY

Xinmin Ge,  
China University of Petroleum (East  
China), China

## REVIEWED BY

Fuyong Wang,  
China University of Petroleum, China  
Likai Cui,  
Northeast Petroleum University, China

## \*CORRESPONDENCE

Yongfei Yang,  
✉ yangyongfei@upc.edu.cn

## SPECIALTY SECTION

This article was submitted to  
Solid Earth Geophysics,  
a section of the journal  
*Frontiers in Earth Science*

RECEIVED 07 December 2022

ACCEPTED 20 February 2023

PUBLISHED 24 March 2023

## CITATION

Yang J, Shan G, Wang Z, Zhang Q, Yang Y  
and Ma W (2023), Experimental study of  
distribution and quantitative  
characterization of discontinuous oil  
phase based on micro-CT.  
*Front. Earth Sci.* 11:1117971.  
doi: 10.3389/feart.2023.1117971

## COPYRIGHT

© 2023 Yang, Shan, Wang, Zhang, Yang  
and Ma. This is an open-access article  
distributed under the terms of the  
[Creative Commons Attribution License  
\(CC BY\)](https://creativecommons.org/licenses/by/4.0/). The use, distribution or  
reproduction in other forums is  
permitted, provided the original author(s)  
and the copyright owner(s) are credited  
and that the original publication in this  
journal is cited, in accordance with  
accepted academic practice. No use,  
distribution or reproduction is permitted  
which does not comply with these terms.

# Experimental study of distribution and quantitative characterization of discontinuous oil phase based on micro-CT

Jiangshan Yang<sup>1</sup>, Gaojun Shan<sup>2</sup>, Zhiqiang Wang<sup>2</sup>, Qi Zhang<sup>1</sup>,  
Yongfei Yang<sup>1\*</sup> and Wenjie Ma<sup>1</sup>

<sup>1</sup>School of Petroleum, China University of Petroleum (East China), Qingdao, China, <sup>2</sup>Research Institute of Exploration and Development of Daqing Oilfield Company Ltd, Daqing, China

When a sandstone reservoir enters the ultra-high water cut stage, the oil phase changes from continuous to discontinuous, which results in difficulties in the further development and utilization of the reservoir. It is important to clarify the flow law and distribution state of discontinuous oil phases to guide the remaining oil production. This study selected samples from sandstone reservoirs, accurately obtained oil and water phase information from digital core, and constructed matrix based on three-dimensional CT scanning to study the law of discontinuous oil phase distribution. We used digital cores to construct pore network models and calculate the pore radius, throat radius, pore-throat ratio, coordination number, and tortuosity to study the influence of pore structure on discontinuous oil phase flow law. A micro-displacement experiment consisting of two phases of simulated reservoir and development was designed. To improve the accuracy of the experiment, the related pressure was controlled to form bound water in the simulated reservoir formation stage. In the simulated reservoir development phase, in situ scanning of cores at different displacement stages was performed to obtain oil and water distributions at different stages in the same location. The number of oil droplets, 3D shape factor, Euler number, and saturation coefficient of the oil phase were calculated, and the micro-remaining oil clumps were quantitatively analyzed. According to the morphology and distribution characteristics, the remaining oil of the discontinuous phase was divided into the types of the throat, film, droplet, island, and corner. The results showed that the sample with a small pore-throat ratio, large coordination number, and small tortuosity was more likely to form dominant channels; moreover, the remaining oil was more concentrated in this state. In the remaining oil of the discontinuous phase, the number of droplets was the largest and had an obvious displacement effect. The island number was small because the selected samples had good connectivity and it is difficult to form large oil droplets in a single pore. In the ultra-high water cut stage, the throat number increased slowly, which was related to the formation of dominant channels. The corner and the film were difficult to displace; thus, their numbers increased steadily. The quantitative characterization of the discontinuous oil phase is helpful for further study of remaining oil at the pore scale.

## KEYWORDS

CT scanning technology, discontinuous oil phase, pore network model, microscopic displacement experiment, quantitative characterization of remaining oil

## Introduction

Sandstone reservoirs have long been the main oil and gas production reservoirs; thus, the interlayer and inner-layer interferences are important challenges in the extraction process (Gao et al., 2016; Thomson et al., 2019). When entering the ultra-high water cut stage, these interferences become more obvious, which brings difficulties to the development of oil and gas reservoirs (Liang et al., 2021; Jiang, 2022). Thus, the study of the distribution of micro-remaining oil in the ultra-high water cut stage is required (Li et al., 2018). In this stage, many continuous oil phases fracture to form discontinuous oil phases distributed as tiny droplets in the pores and throat (Grattoni and Dawe, 2003; Meybodi et al., 2011; Li et al., 2017; Ding et al., 2018; Sun et al., 2021). The study of the flow law and distribution of these tiny oil droplets has important guiding significance for improving the overall reservoir recovery.

Microphysical experiments and numerical simulations are commonly used to study micro-remaining oil distribution (Guo et al., 2015; Huang et al., 2018; Yang et al., 2022). The physical experiments on remaining oil mainly include micro- and macro-experiments (Jing et al., 2021; Jiang et al., 2022). Many methods have been applied to study the micro-remaining oil through micro-experiments, including scanning electron microscopy, micro-CT scanning, and nuclear magnetic resonance imaging (Rosestolato et al., 2019; Zhang et al., 2021; Lu et al., 2022). The advantages of micro-CT scanning, such as its high precision and high resolution have made this technology an important tool for research on remaining oil (Liu et al., 2017; Yang et al., 2021). Combined with pore-scale modeling (Golparvar et al., 2018; Yang and Zhou, 2021), digital cores and pore network models based on real cores can be obtained (Liu et al., 2014; Wang et al., 2019). Using pore network models, the number and radius of pore throats can be calculated and the pore-throat structure can be evaluated based on the pore coordination number, tortuosity, and other parameters (An et al., 2016; Oluwadebi et al., 2019; Thomson et al., 2020; Wang X. et al., 2021).

Research has also focused on the distribution of remaining oil in different development stages (Yue et al., 2018; Zhang S. et al., 2019; Wang Y. et al., 2021). To explore the distribution of microscopic remaining oil in physical experiments, digital cores are widely used (Yang et al., 2016; Guo et al., 2018; Lei et al., 2021). Image processing of micro-CT scan data can be used to construct 3D digital cores that accurately divide the oil and water phases, as well as particles (Kornilov et al., 2020). The remaining oil distribution can be visualized by processing oil phase information. Based on the digital core, the volume, surface area, shape factor, and other parameters of the micro-remaining oil can be calculated for the quantitative analysis of the remaining oil characteristics (Liu et al., 2013; Hu et al., 2017; Cheng et al., 2021). Combining shape factor, Euler number, and other parameters, researchers have quantitatively characterized micro-remaining oil (Feng et al., 2014; Sun et al., 2017). These parameters are especially helpful for the study of discontinuous microscopic remaining oil (Ding et al., 2018; Hou et al., 2019). Combined with pore structure analysis and quantitative analysis of microscopic remaining oil, a true and accurate analysis of the remaining oil research of the reservoir can be made (Zhong et al., 2021; Tong et al., 2022).

The present investigation selected sandstone reservoir samples to study the distribution of the microscopic remaining oil in the ultra-high water cut stage and quantitatively analyzed the characteristics of the discontinuous oil phase. Experimentally, we

designed two stages of simulated reservoir formation and development to make the experimental results as accurate as possible. Using micro-CT scanning, we analyzed the pore-throat structure of the samples based on the pore network and quantitatively described the micro-remaining oil based on the digital core. Finally, we summarized the effect of pore-throat structure on the distribution of micro-remaining oil and quantitatively characterized the discontinuous oil phase. The results of this study provide an important reference for the further study of the microscopic remaining oil in sandstone reservoirs, especially the discontinuous oil phase.

## Experimental materials and methods

### Materials and equipment

X-rays are penetrative. When they pass through different media, different amounts of energy are absorbed. The reverse calculation of the attenuated X-rays allows the differentiation of different media. CT scanning passes X-rays through a sample and applies energy attenuation to compute the density distribution and determine the internal structure of the sample (Wang et al., 2013). A MicroCT-400 (Zeiss) was used to perform the CT experiments. X-ray attenuation conforms to the Beer-Lambert law (Swinehart, 1962):

$$I = I_0 e^{-\sum_i \mu_i x_i}, \quad (1)$$

where  $I_0$  is the initial ray energy strength,  $I$  is the receiving ray energy strength,  $\mu_i$  is the attenuation coefficient of the medium, and  $x_i$  is the length of the medium.

In this experiment, three cores from real sandstone reservoirs were selected. We processed the samples into standard samples with a diameter of 2.5 cm and tested the effective porosity and absolute permeability of each sample. The effective porosity values of the three samples were 24.73%, 26.17%, and 28.18%, respectively. Also, the absolute permeability values of three samples were  $1.089 \mu\text{m}^2$ ,  $1.573 \mu\text{m}^2$ , and  $2.103 \mu\text{m}^2$ , respectively.

According to the original formation fluid environment of the samples, a simulated formation oil with a density of  $0.8 \text{ g/cm}^3$  and viscosity of  $9.6 \text{ mPa} \cdot \text{s}$  was prepared using white oil and kerosene. The simulated formation water was also prepared, with a density of  $1.08 \text{ g/cm}^3$ , viscosity of  $0.65 \text{ mPa} \cdot \text{s}$ , salinity of  $6,778 \text{ mg/L}$ , and an oil-water interfacial tension of  $36 \text{ mN/m}$  using distilled water and potassium iodide. The sample was placed in a gripper made of Polyether Ether Ketone Resin (PEEK). This material had good X-ray transmittance, which can produce better scanning results. Microflow pumps, intermediate vessels, pressure pumps, and other equipment were also used.

### Experimental steps

To ensure the accuracy of the results of the micro-displacement experiments, the experiment consisted of two parts: simulated reservoir formation and simulated reservoir development. Most previous experiments ignored the impact of irreducible water (Yang et al., 2020). Unavoidably, irreducible

water affects the experiment analysis. In contrast, the experiments in the present study considered the effect of irreducible water. Before the experiment started, the samples were processed to a length of about 1.5 cm and a diameter of 0.5 cm, to calculate the Pore Volume (PV) according to the corresponding effective porosity.

During the simulated reservoir formation phase, the samples were dried to ensure that no liquid phase was present inside the sample. The samples were then placed in a gripper, injected with simulated formation water, and maintained at a pressure of 4 MPa for 1 hour to ensure that the simulated formation water fully entered the micro-pores. The simulated formation oil was then injected to simulate reservoir formation, at a pressure of 3 MPa for 1 hour. By controlling the pressure between the two stages, irreducible water was constructed to some extent. In this stage, three scanning nodes were set, corresponding to dry sample, saturated water, and saturated oil. The three scans were compared to observe the structure of the irreducible water. Three scanning nodes, waterflooding 1 PV, waterflooding 5 PV, and waterflooding 30 PV, were also set in the simulated reservoir formation stage. Among them, waterflooding 1 PV corresponded to the middle water-cut stage, waterflooding 5 PV to the high water-cut stage, and waterflooding 30 PV to the ultra-high water-cut stage.

The entire experimental process was performed at 20°C, with atmospheric pressure at the outlet during displacement.

## Pore network model

After CT scans were performed of the dry core sample, the grayscale images inside the samples were displayed. The rock skeleton and pores in the images were identified using an algorithm to allow binary processing of the grayscale images. The digital core was obtained after two-dimensional data reconstruction (Gao et al., 2014). The combination of digital cores and binarized images can be used to extract the internal space of the sample. The pores and throats can then be identified using an algorithm. The pore network model is obtained by optimizing the data. Pore network models obtained based on real cores can truly show the internal structure of the sample. Through the pore network model, we calculated the pore radius, throat radius, pore-throat ratio, coordination number, and tortuosity. The coordination number was used to display the number of throats connected to the pores and to describe the connectivity of the pore-throat. The tortuosity is the ratio of the distance between the real flow of fluid to the straight-line distance and is used to describe the twists and turns inside the sample.

## Pore-scale classification of remaining oil

The CT scanning of the waterflooding stages provided information on the forms and distribution of the oil and water phases. Three-dimensional data of the oleic and aqueous phases can be obtained by reconstruction of the two-dimensional scanning data. We can then calculate the surface area, cross-sectional area, and volume of the oleic and aqueous phases. According to the number of pores occupied by the remaining, the three-dimensional shape factor, Euler number 3D, and saturation coefficient can be used for the quantitative analysis of the remaining oil clusters.

The three-dimensional shape factor was used to describe the circularity of the remaining oil in the three-dimensional space (Prodanović et al., 2007), which is given by

$$G = \frac{6\sqrt{\pi}V}{S^{1.5}}, \quad (2)$$

where  $G$  is the three-dimensional shape factor,  $V$  is the volume of a single oil cluster (in  $\mu\text{m}^3$ ), and  $S$  is the surface area of a single oil cluster (in  $\mu\text{m}^2$ ).

The 3D Euler number was used to describe the complexity and connectivity of the remaining oil form (Hirzebruch and Höfer, 1990), which is given by

$$E_N = \beta_0 - \beta_1 + \beta_2, \quad (3)$$

where  $\beta_0$  is the number of pores occupied by a single oil cluster,  $\beta_1$  is the connectivity, and  $\beta_2$  is the number of enclosed cavities.

In this step, the concept of oil droplet saturation coefficient is introduced, which is the ratio of oil droplet volume to pore volume in the pore. The saturation coefficient is used to describe the index of a single oil cluster occupying the pore volume, which is given by

$$P = \frac{V}{V_p}, \quad (4)$$

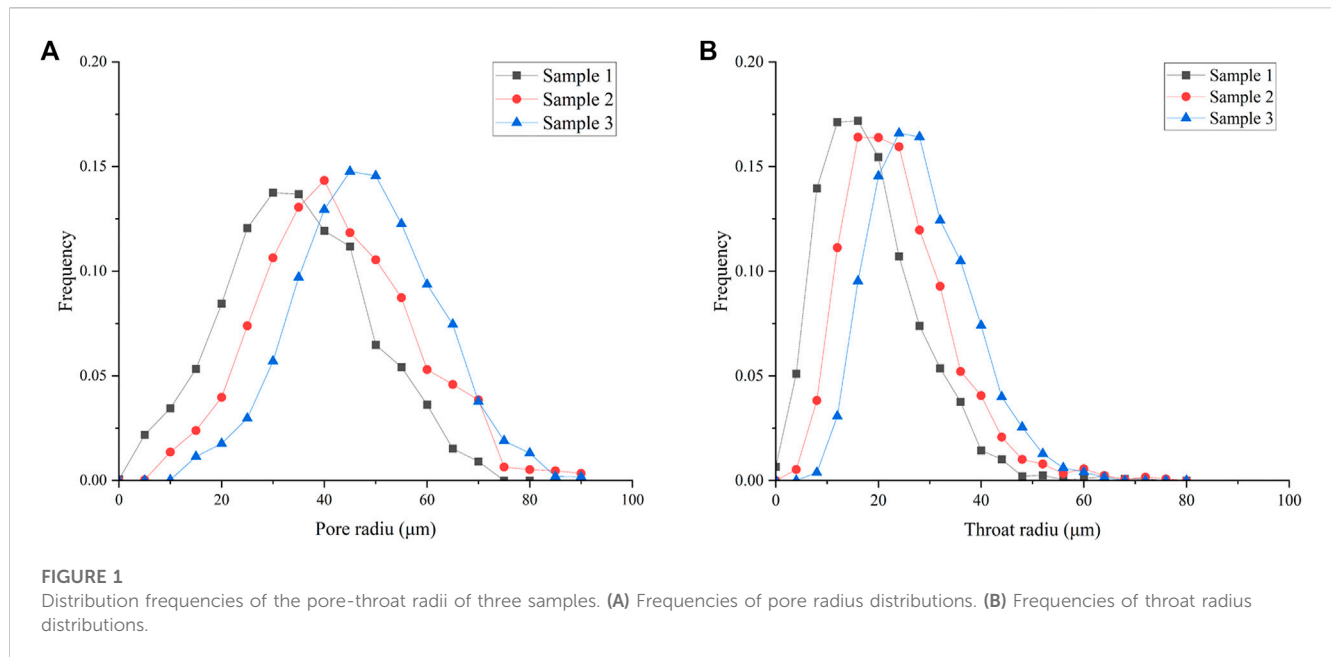
where  $P$  is the saturation coefficient,  $V$  is the volume of a single oil cluster, and  $V_p$  is the pore volume occupied by the single oil cluster.

## Results

### Analysis of pore-throat structures

After processing the scanning results of the three dry samples, three digital cores were obtained, which contained information on pore and particle phases. The pore phase information was extracted, and the pore network model was established using the Lee-Kashyap-Chu method (Lee et al., 1994). In this method, the central axis system of the pore structure is first established. The central axis is then modified several times to ensure that it accurately represents the pore structure of the core. The center position of each pore is located on the optimized central axis, and the pore space is divided into the pore and throat to obtain the final pore network model (Zhang L. et al., 2019). Using the pore network model, the pore and throat radii can be calculated. The probability distributions of the pore and throat radii were obtained by counting the numbers of pore and throat radii (Figure 1). The frequency trends of the pore radii of the three samples were similar (Figure 1A). The pore radius of the sample with low permeability was relatively small. The frequency distribution trends of the throat radii of the three samples were also similar; however, the size distribution was more concentrated (Figure 1B).

According to the pore and throat radii, the average pore-throat radius ratio of the sample was calculated. The average pore-throat radius ratio, pore coordination number, and tortuosity of the three samples were also calculated. The pore-throat radius ratio is an important parameter affecting permeability; the pore-throat radius ratios of the three samples were 2.10, 2.11, and 2.19, respectively. The average coordination numbers, which describe the average number of throats per pore connection, were 2.02, 2.20, and



2.52 for the three samples, respectively. Tortuosity is the ratio of the true length of the flow path from the sample to the linear distance, which describes the complexity of the pore-throat structure. The tortuosity values of the three samples were 1.73, 1.71, and 1.63, respectively.

## Analysis of the displacement experiment results

Digital cores containing information on the water, oil, and particle phases were obtained after processing the CT images of each scanning node in the micro-displacement experiment. In the simulated reservoir formation stage, the irreducible water was successfully constructed by controlling the pressure. The irreducible water saturation pairs of the three samples were 34.5%, 33.6%, and 32.5%, respectively. The reservoir-bound irreducible saturation of the three samples ranged from 30% to 35%. As the bound water-saturated of the experimental structure is also in this range, this experiment was more meaningful for reference. In the simulated reservoir formation stage, the visualization of oil and water phases in the digital core can be used to obtain the microscopic remaining oil distributions at different displacement times (Figure 2). According to the effect of water injection, Sample 3 was more likely to form a dominant channel (Figure 2C). When the dominant channel forms in the sample, the remaining oil in other non-dominant channel locations is relatively more concentrated. Because the pore-throat radius ratio was the largest and the coordination number was small in Sample 1, the remaining oil was difficult to displace and the proportion of remaining oil was larger (Figure 2A). Most of the isolated micro-remaining oil existed in the discontinuous oil phase. Sample 2 showed a medium condition (Figure 2B).

According to the scale characteristics of the micro-remaining oil, the remaining oil can be divided into the network, multiples,

and singles (Figure 3). The network is characterized by occupying a large area of pore space with a large volume, multiples are characterized by occupying two or more pores, and singles are characterized by occupying one pore or sharing a pore with other remaining oil. In the ultra-high water cut stage, the proportion of single remaining oil increases and exists in each pore as discontinuous oil phase dispersion. These tiny oil droplets are small, numerous, and complex. The remaining oil can be classified as throat, film, droplet, island, and corner based on shape, Euler number, and oil droplet saturation coefficient. Throats existed in the channel between two pores. Films were attached to the wall of the pore or throat. Droplets existed in the pores and occupied less pore space. Islands also existed in the pores but occupied more pore space. Corners existed in the blind end or corner of the pores.

## Quantitative characterization of the remaining oil

The quantitative characterization of the microscopic remaining oil was performed based on the analysis of the results of the displacement experiments (Figure 4). The number and type of single remaining oils were large, and the volume proportions were small. Therefore, the remaining oil in the network, as well as the multiple and single forms, were analyzed first. The volume proportions of remaining oil in the three samples in different periods showed the same trends. The volume proportion of the single remaining oil in Sample 1 changed more than the proportions in samples 2 and 3 due to the pore-throat structure of the sample. A larger pore-throat ratio and smaller pore coordination number are conducive to the formation of single remaining oil. After waterflooding at 30 PV, Sample 3 showed the largest proportion of the network's remaining oil volume. This may be related to the fact that Sample 3 was more

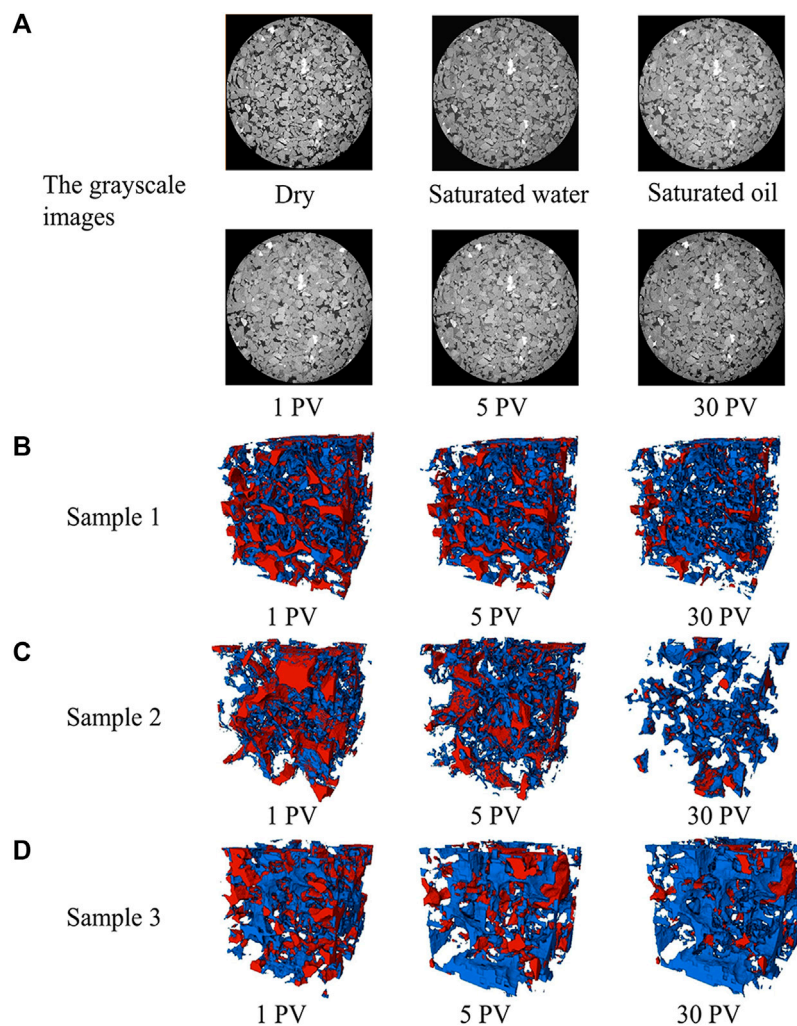


**FIGURE 2**

(A) Grayscale images of Sample 1, including the comparison of the CT grayscale images of the dry core, saturated formation water, saturated oil, and different stages of fluid displacement. (B) Visualization of the oil–water distribution in Sample 1, including the oil (red) and water (blue) phases in waterflooding at 1 PV, 5 PV, and 30 PV. (C–D) Visualizations of the oil–water distributions in samples 2 and 3, respectively.

likely to form the dominant channel, leading to the relative accumulation of remaining oil in the non-dominant channel. All data from Sample 2 were medium.

The distribution of micro-remaining oil becomes more complicated after the continuous phase is broken into the discontinuous phase. The throat exists in the narrow channel between two pores. Due to capillary forces, the remaining oil contracts toward the middle of the throat and is difficult to displace. The number of throats increased during waterflooding from 1 PV to 5 PV compared to waterflooding from 5 PV to 30 PV. The films were attached to the pore and throat wall in large numbers. The droplets existed in pores and were the most abundant of the five types of single remaining oil. The increment of this number decreased at 30 PV of waterflooding, possibly because the numbers of droplets formed by the network and the multiple remaining oil fracture were lower and easier to displace at this stage. The islands occupied larger spaces in the pores and were

difficult to displace. The corners existed in the blind ends and pore corners and were the most difficult to displace.

## Discussion

This study selected three sandstone samples with different permeability. CT scanning and digital core technology were used to study the pore-throat structure of these samples and the micro-remaining oil distributions at different waterflooding stages. According to the distribution and morphological characteristics, the micro-remaining oil was quantitatively characterized and the discontinuous remaining oil was studied in detail. The results were as follows.

- (1) The samples with high permeability, small pore-throat ratio, and pore coordination number were more likely to form

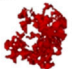






| Classification | Typical figure  | Standards                                | Distribution Features                                     |
|----------------|---|--|---|
| Network        |  | $G < 0.3$                                | Occupy a large area of pore space, a large volume         |
| Multiple       |  | $E_N \geq 1$<br>$0.3 < G < 0.7$          | Occupy two or more pores                                  |
| Throat         |  | $E_N < 1, P > 0.5$<br>$G > 0.7, E_N < 1$ |   |
| Film           |  | $E_N < 1, P < 0.5$<br>$G > 0.7, E_N < 1$ |   |
| Droplet        |  | $0.2 < P < 0.7$<br>$G > 0.7, E_N < 1$    | The single, occupy one pore or share the pore with others |
| Island         |  | $P > 0.7$<br>$G > 0.7, E_N < 1$          |   |
| Corner         |  | $P < 0.2$                                |   |

FIGURE 3 Quantitative characterization of micro-remaining oil.

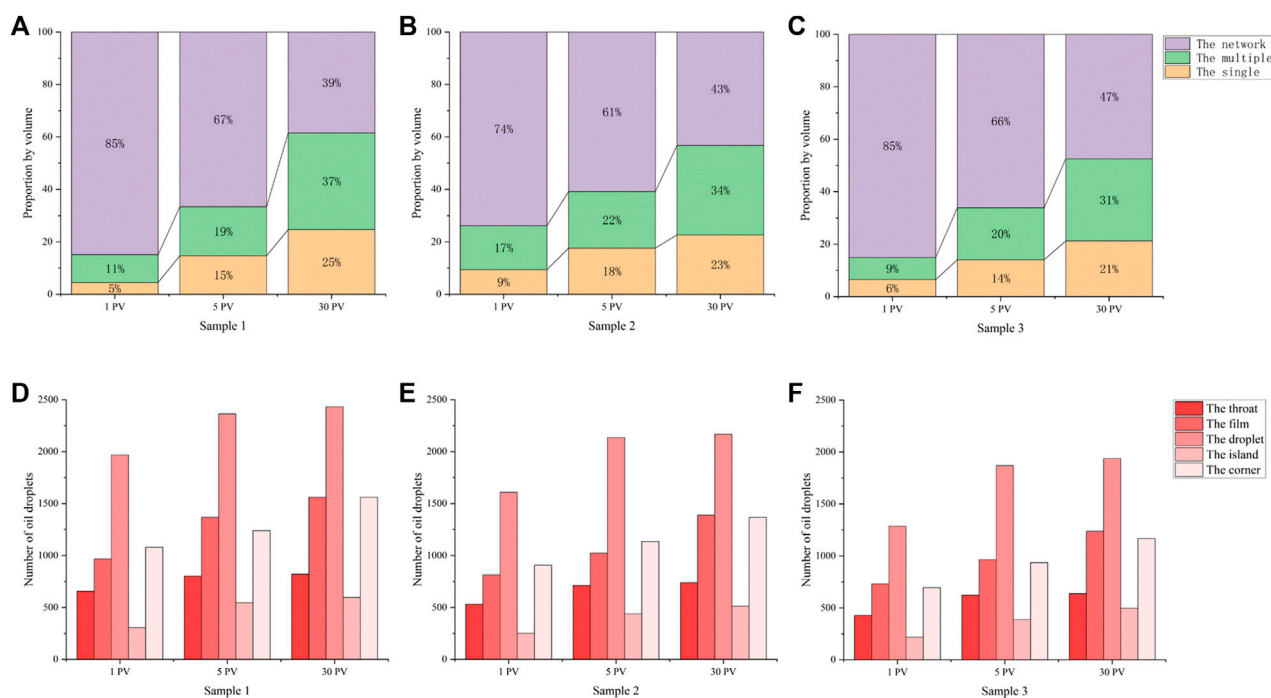


FIGURE 4 Changes in micro-remaining oil during waterflooding. (A–C) Changes in the volume proportion of the network, the multiple, and the single. (D–F) Changes in throat, film, droplet, island, and corner numbers.

dominant channels during waterflooding. In the case of waterflooding at 30 pv, the volume proportion of the network’s remaining oil was the largest in Sample 3. This

occurred because the remaining oil in the non-dominant channel area was relatively more concentrated after the formation of the dominant channel. There was also a close

relationship between the micro-remaining oil distribution and the pore-throat structure.

- (2) Throughout the displacement experiments, the variation trends for each type of remaining oil in the three samples were similar. The volume proportion of the network was constantly decreasing, while the volume proportions of the multiple and the single were constantly increasing because the network's remaining oil broke off to form the multiple and single remaining oils. The single remaining oil was the discontinuous oil phase, which showed the largest increment in Sample 1. This was related to the larger pore-throat ratio of Sample 1. Moreover, in a complex pore-throat structure, the continuous oil phase was more likely to fracture to form a discontinuous oil phase.
- (3) The remaining oil droplets were quantitatively analyzed according to their morphology and attachment. The throat remaining oil existed in an elongated form in the channel between the two pores, with a slow increase in number after the formation of the dominant channel. The film was attached to the pore and throat wall in a flat form and more easily formed in samples with large pore-throat radii. The morphologies of the droplet and the island's remaining oil were similar, with the main difference being that they occupied different pore space sizes. For waterflooding at 30 pv, the increment of the droplet remaining oil decreased by 20%. The corner remaining oil was mainly absorbed in the blind end of the pores, where it was difficult to displace; thus, the number of corners with remaining oil increased steadily.

## Data availability statement

The raw data supporting the conclusion of this article will be made available by the authors, without undue reservation.

## References

- An, S., Yao, J., Yang, Y., Zhang, L., Zhao, J., and Gao, Y. (2016). Influence of pore structure parameters on flow characteristics based on a digital rock and the pore network model. *J. Nat. Gas Sci. Eng.* 31, 156–163. doi:10.1016/j.jngse.2016.03.009
- Cheng, B., Li, J., Jiang, S., Lu, C., Su, H., Yu, F., et al. (2021). Pore-scale investigation of microscopic remaining oil variation characteristic in different flow rates using micro-CT. *Energies* 14 (11), 3057. doi:10.3390/en14113057
- Ding, S., Jiang, H., and Xi, Y. (2018). The micromechanical cause and pore selection mechanism of remaining oil at ultra-high water cut period. *J. Liaoning Univ. Petroleum Chem. Technol.* 38 (1), 45–49. doi:10.3969/j.issn.1672-6952.2018.01.008
- Feng, C., Bao, Z., Yang, L., Si, X., Guibin, X., and Xiong, H. (2014). Reservoir architecture and remaining oil distribution of deltaic front underwater distributary channel. *Petroleum Explor. Dev.* 41 (3), 358–364. doi:10.1016/s1876-3804(14)60040-9
- Gao, P., Jiang, C., Huang, Q., Cai, H., Luo, Z., and Liu, M. (2016). Fluvial facies reservoir productivity prediction method based on principal component analysis and artificial neural network. *Petroleum* 2 (1), 49–53. doi:10.1016/j.petlm.2015.12.005
- Gao, Y., Yao, J., Yang, Y., and Zhao, J. (2014). "REV identification of tight sandstone in sulige gas field in changqing oilfield China using CT based digital core technology," in Paper SCA2014-036 Presented at the 2014 International Symposium of the Society of Core Analysts, Avignon, France, 8–11.
- Golparvar, A., Zhou, Y., Wu, K., Ma, J., and Yu, Z. (2018). A comprehensive review of pore scale modeling methodologies for multiphase flow in porous media. *Adv. Geo-Energy Res.* 2 (4), 418–440. doi:10.26804/ager.2018.04.07
- Grattoni, C. A., and Dawe, R. A. (2003). Gas and oil production from waterflood residual oil: Effects of wettability and oil spreading characteristics. *J. Pet. Sci. Eng.* 39 (3-4), 297–308. doi:10.1016/s0920-4105(03)00070-6
- Guo, C., Wang, X., Wang, H., He, S., Liu, H., and Zhu, P. (2018). Effect of pore structure on displacement efficiency and oil-cluster morphology by using micro-computed tomography ( $\mu$ CT) technique. *Fuel* 230, 430–439. doi:10.1016/j.fuel.2018.05.058
- Guo, C., Xu, J., Wei, M., and Jiang, R. (2015). Experimental study and numerical simulation of hydraulic fracturing tight sandstone reservoirs. *Fuel* 159, 334–344. doi:10.1016/j.fuel.2015.06.057
- Hirzebruch, F., and Höfer, T. (1990). On the Euler number of an orbifold. *Math. Ann.* 286, 255–260. doi:10.1007/bf01453575
- Hou, J., Wu, D., Wei, B., Zhou, K., Gong, L., Cao, X., et al. (2019). Percolation characteristics of discontinuous phase and mechanisms of improving oil displacement efficiency in heterogeneous composite flooding. *J. China Univ. Petroleum Ed. Nat. Sci.* 43 (5), 128–135. doi:10.3969/j.issn.1673-5005.2019.05.014
- Hu, W., Lv, C., Wang, R., Yang, Y., and Wang, X. (2017). Mechanism of CO<sub>2</sub> immiscible flooding and distribution of remaining oil in water drive oil reservoir. *Editor. Dep. Petroleum Geol. Recovery Effic.* 24 (5), 99–105. doi:10.13673/j.cnki.cn37-1359/te.2017.05.015
- Huang, S., Wu, Y., Meng, X., Liu, L., and Ji, W. (2018). Recent advances on microscopic pore characteristics of low permeability sandstone reservoirs. *Adv. Geo-Energy Res.* 2 (2), 122–134. doi:10.26804/ager.2018.02.02
- Jiang, N., Zhang, Z., Qu, G., Zhi, J., and Zhang, R. (2022). Distribution characteristics of micro remaining oil of class III reservoirs after fracture flooding in daqing oilfield. *Energies* 15 (9), 3385. doi:10.3390/en15093385
- Jiang, X. (2022). "Comprehensive development strategies of water-flooding for multilayer sandstone oilfield in the late period of ultra high water cut," in International Field Exploration and Development Conference (Springer), 2874–2881.

## Author contributions

JY contributed to the study conception and design. GS and ZW organized the database. QZ and WM performed the statistical analysis. YY contributed to the manuscript revision and read and approved the submitted version.

## Funding

We express our appreciation to the following for providing financial support: the National Natural Science Foundation of China (Nos 52034010 and 52288101), the Shandong Provincial Natural Science Foundation (No. ZR2019JQ21), and the Program for Changjiang Scholars and Innovative Research Team in University (IRT\_16R69).

## Conflict of interest

Authors GS and ZW were employed by the Daqing Oilfield Company Ltd. The remaining authors declare that the research was conducted in the absence of any commercial or financial relationships that could be construed as a potential conflict of interest.

The editor [XG] and the reviewer [FW] declared a shared affiliation with the authors [JY, QZ, YY, and WM] at the time of review.

## Publisher's note

All claims expressed in this article are solely those of the authors and do not necessarily represent those of their affiliated organizations, or those of the publisher, the editors, and the reviewers. Any product that may be evaluated in this article, or claim that may be made by its manufacturer, is not guaranteed or endorsed by the publisher.

- Jing, W., Fu, S., Zhang, L., Li, A., Ren, X., Xu, C., et al. (2021). Pore scale experimental and numerical study of surfactant flooding for enhanced oil recovery. *J. Pet. Sci. Eng.* 196, 107999. doi:10.1016/j.petrol.2020.107999
- Kornilov, A., Reimers, I., Safonov, I., and Yakimchuk, I. (2020). Visualization of quality of 3D tomographic images in construction of digital rock model. *Sci. Vis.* 12 (1), 70–82. doi:10.26583/sv.12.1.06
- Lee, T. C., Kashyap, R. L., and Chu, C. N. (1994). Building skeleton models via 3-D medial surface axis thinning algorithms. *CVGIP Graph. Models Image Process.* 56 (6), 462–478. doi:10.1006/cgip.1994.1042
- Lei, Q., Zhang, L., Tang, H., Zhao, Y., Chen, M., and Xie, C. (2021). Quantitative study of different patterns of microscale residual water and their effect on gas permeability through digital core analysis. *J. Pet. Sci. Eng.* 196, 108053. doi:10.1016/j.petrol.2020.108053
- Li, J., Jiang, H., Wang, C., Zhao, Y., Gao, Y., Pei, Y., et al. (2017). Pore-scale investigation of microscopic remaining oil variation characteristics in water-wet sandstone using CT scanning. *J. Nat. Gas Sci. Eng.* 48, 36–45. doi:10.1016/j.jngse.2017.04.003
- Li, J., Liu, Y., Gao, Y., Cheng, B., Fanle, M., and Huaimin, X. (2018). Effects of microscopic pore structure heterogeneity on the distribution and morphology of remaining oil. *Petroleum Explor. Dev.* 45 (6), 1112–1122. doi:10.1016/s1876-3804(18)30114-9
- Liang, Y., Liang, W., He, W., and Li, Z. (2021). Response to the variation of clay minerals during ASP flooding in the saertu oilfield in the songliao basin. *Front. Earth Sci.* 1017. doi:10.3389/feart.2021.764052
- Liu, X., Zhu, H., and Liang, L. (2014). Digital rock physics of sandstone based on micro-CT technology. *Chinese J. Geophys.* 57 (4), 1133–1140. doi:10.6038/cjg20140411
- Liu, Y. K., Cai, L. Z., Chen, L. Y., and Wang, F. J. (2013). Research on microscopic characteristics of remaining oil distribution after strong alkali ASP flooding by laser scanning confocal technology. *Adv. Mater. Res.* 616–618, 757–761. doi:10.4028/www.scientific.net/amr.616-618.757
- Liu, Z., Yang, Y., Yao, J., Zhang, Q., Ma, J., and Qian, Q. (2017). Pore-scale remaining oil distribution under different pore volume water injection based on CT technology. *Adv. Geo-Energy Res.* 1 (3), 171–181. doi:10.26804/ager.2017.03.04
- Lu, Y., Liu, D., Cai, Y., Li, Q., and Zhou, Y. (2022). Spontaneous imbibition in coal with *in-situ* dynamic micro-CT imaging. *J. Pet. Sci. Eng.* 208, 109296. doi:10.1016/j.petrol.2021.109296
- Meybodi, H. E., Kharrat, R., and Araghi, M. N. (2011). Experimental studying of pore morphology and wettability effects on microscopic and macroscopic displacement efficiency of polymer flooding. *J. Pet. Sci. Eng.* 78 (2), 347–363. doi:10.1016/j.petrol.2011.07.004
- Oluwadebi, A. G., Taylor, K. G., and Ma, L. (2019). A case study on 3D characterisation of pore structure in a tight sandstone gas reservoir: The collyhurst sandstone, east Irish sea basin, northern england. *J. Nat. Gas Sci. Eng.* 68, 102917. doi:10.1016/j.jngse.2019.102917
- Prodanović, M., Lindquist, W., and Seright, R. (2007). 3D image-based characterization of fluid displacement in a Berea core. *Adv. Water Resour.* 30 (2), 214–226. doi:10.1016/j.advwatres.2005.05.015
- Roselotolo, J. C., Pérez-Gramatges, A., Lachter, E. R., and Nascimento, R. S. (2019). Lipid nanostructures as surfactant carriers for enhanced oil recovery. *Fuel* 239, 403–412. doi:10.1016/j.fuel.2018.11.027
- Sun, H., Zhao, Y., and Yao, J. (2017). Micro-distribution and mechanical characteristics analysis of remaining oil. *Petroleum* 3 (4), 483–488. doi:10.1016/j.petlm.2017.03.005
- Sun, P., Xu, H., Zhu, H., Jia, L., Hu, X., Fang, H., et al. (2021). Investigation of pore-type heterogeneity and its control on microscopic remaining oil distribution in deeply buried marine clastic reservoirs. *Mar. Petroleum Geol.* 123, 104750. doi:10.1016/j.marpetgeo.2020.104750
- Swinehart, D. F. (1962). The beer-lambert law. *J. Chem. Educ.* 39 (7), 333. doi:10.1021/ed039p333
- Thomson, P.-R., Ellis, R., Chiarella, D., and Hier-Majumder, S. (2020). Microstructural analysis from X-Ray CT images of the brae formation sandstone, North Sea. *Front. Earth Sci.* 246. doi:10.3389/feart.2020.00246
- Thomson, P.-R., Hazel, A., and Hier-Majumder, S. (2019). The influence of microporous cements on the pore network geometry of natural sedimentary rocks. *Front. Earth Sci.* 7, 48. doi:10.3389/feart.2019.00048
- Tong, Q., He, D., Xia, Z., Huang, J., Di, K., Xu, F., et al. (2022). Influence of reservoir pore-throat structure heterogeneity on water-flooding seepage: A case study of yanchang formation in ordos basin. *Minerals* 12 (10), 1243. doi:10.3390/min12101243
- Wang, C., Yao, J., Yang, Y., and Wang, X. (2013). Study on resolution selection for digital rock construction with CT scanning method. *Sci. Technol. Eng.* 13, 1671–1815. doi:10.3969/j.issn.1671-1815.2013.04.043
- Wang, X., Yin, H., Zhao, X., Li, B., and Yang, Y. (2019). Microscopic remaining oil distribution and quantitative analysis of polymer flooding based on CT scanning. *Adv. Geo-Energy Res.* 3 (4), 448–456. doi:10.26804/ager.2019.04.10
- Wang, X., Zhang, Z., Gong, R., and Wang, S. (2021). Pore network modeling of oil–water flow in jimsar shale oil reservoir. *Front. Earth Sci.* 9, 738545. doi:10.3389/feart.2021.738545
- Wang, Y., Liu, H., Guo, M., Shen, X., Han, B., and Zhou, Y. (2021). Image recognition model based on deep learning for remaining oil recognition from visualization experiment. *Fuel* 291, 120216. doi:10.1016/j.fuel.2021.120216
- Yang, Y., Cai, S., Yao, J., Zhong, J., Zhang, K., Song, W., et al. (2021). Pore-scale simulation of remaining oil distribution in 3D porous media affected by wettability and capillarity based on volume of fluid method. *Int. J. Multiph. Flow* 143, 103746. doi:10.1016/j.ijmultiphaseflow.2021.103746
- Yang, Y., Tao, L., Iglauer, S., Hejazi, S. H., Yao, J., Zhang, W., et al. (2020). Quantitative statistical evaluation of micro residual oil after polymer flooding based on X-ray micro computed-tomography scanning. *Energy & Fuels* 34 (9), 10762–10772. doi:10.1021/acs.energyfuels.0c01801
- Yang, Y., Xu, Q., Li, X., Zhang, L., Lan, X., Wang, J., et al. (2022). Pore-scale simulation of gas-water two-phase flow in volcanic gas reservoir based on Volume of Fluid method. *J. Nat. Gas Sci. Eng.* 106, 104733. doi:10.1016/j.jngse.2022.104733
- Yang, Y., Zhou, Y., Blunt, J. B., Yao, J., and Cai, J. (2021). Advances in multiscale numerical and experimental approaches for multiphysics problems in porous media. *Adv. Geo-Energy Res.* 5 (3), 233–238. doi:10.46690/AGER.2021.03.01
- Yang, Y., Zhang, W., Gao, Y., Wan, Y., Su, Y., An, S., et al. (2016). Influence of stress sensitivity on microscopic pore structure and fluid flow in porous media. *J. Nat. Gas Sci. Eng.* 36, 20–31. doi:10.1016/j.jngse.2016.09.061
- Yue, M., Zhu, W., Han, H., Song, H., Long, Y., and Lou, Y. (2018). Experimental research on remaining oil distribution and recovery performances after nano-micron polymer particles injection by direct visualization. *Fuel* 212, 506–514. doi:10.1016/j.fuel.2017.10.055
- Zhang, L., Jing, W., Yang, Y., Yang, H., Guo, Y., Sun, H., et al. (2019). The investigation of permeability calculation using digital core simulation technology. *Energies* 12 (17), 3273. doi:10.3390/en12173273
- Zhang, S., Yang, M., Kang, Z., Liu, Z., Long, X., Kunyan, L., et al. (2019). Controlling factors of remaining oil distribution after water flooding and enhanced oil recovery methods for fracture-cavity carbonate reservoirs in Tahe Oilfield. *Petroleum Explor. Dev.* 46 (4), 786–795. doi:10.1016/s1876-3804(19)60236-3
- Zhang, X., Wei, B., You, J., Liu, J., Wang, D., Lu, J., et al. (2021). Characterizing pore-level oil mobilization processes in unconventional reservoirs assisted by state-of-the-art nuclear magnetic resonance technique. *Energy* 236, 121549. doi:10.1016/j.energy.2021.121549
- Zhong, X., Zhu, Y., Jiao, T., Qi, Z., Luo, J., Xie, Y., et al. (2021). Microscopic pore throat structures and water flooding in heterogeneous low-permeability sandstone reservoirs: A case study of the jurassic yan'an formation in the huanjiang area, ordos basin, northern China. *J. Asian Earth Sci.* 219, 104903. doi:10.1016/j.jseas.2021.104903